Anomalous diffusion, spatial coherence, and viscoelasticity from the energy landscape of human chromosomes

Michele Di Pierro[a,1,2], Davit A. Potoyan[b,1], Peter G. Wolynes[a,c,d,e], and José N. Onuchic[a,c,d,e,2]

[a]Center for Theoretical Biological Physics, Rice University, Houston, TX 77005; [b]Department of Chemistry, Iowa State University, Ames, IA 50011; [c]Department of Chemistry, Rice University, Houston, TX 77005; [d]Department of Physics & Astronomy, Rice University, Houston, TX 77005; and [e]Department of Biosciences, Rice University, Houston, TX 77005

Contributed by José N. Onuchic, June 8, 2018 (sent for review April 12, 2018; reviewed by Olga K. Dudko and Andrew J. Spakowitz)

The nucleus of a eukaryotic cell is a nonequilibrium system where chromatin is subjected to active processes that continuously rearrange it over the cell's life cycle. Tracking the motion of chromosomal loci provides information about the organization of the genome and the physical processes shaping that organization. Optical experiments report that loci move with subdiffusive dynamics and that there is spatially coherent motion of the chromatin. We recently showed that it is possible to predict the 3D architecture of genomes through a physical model for chromosomes that accounts for the biochemical interactions mediated by proteins and regulated by epigenetic markers through a transferable energy landscape. Here, we study the temporal dynamics generated by this quasi-equilibrium energy landscape assuming Langevin dynamics at an effective temperature. Using molecular dynamics simulations of two interacting human chromosomes, we show that the very same interactions that account for genome architecture naturally reproduce the spatial coherence, viscoelasticity, and the subdiffusive behavior of the motion in interphase chromosomes as observed in numerous experiments. The agreement between theory and experiments suggests that even if active processes are involved, an effective quasi-equilibrium landscape model can largely mimic their dynamical effects.

chromatin dynamics | anomalous diffusion | genome architecture | phase separation | dynamically associated domains

The nucleus of a eukaryotic cell is an active environment where ATP-driven molecular machines act in conjunction with the ordinary thermal fluctuations of Brownian motion to create specific structures and nontrivial dynamical properties (1). The dynamics of the nuclear material is important for cell functioning since the chromosomal DNA completely rearranges as the cell proceeds through the phases of its life cycle. Additionally, in each of these phases the dynamic reorganization of chromosomes seems to be involved in ongoing biological processes, such as transcription, replication, recombination, and segregation. Tracking the motion of chromosomal loci provides relevant information about the physical processes driving the movements of DNA along with its various associated proteins and RNAs in the crowded nuclear environment (2–4). Experiments suggest that genomic loci do not diffuse freely but instead follow a random walk that has a scaling exponent that differs from that predicted by the simplest polymer dynamics models (2). In addition to the observed subdiffusivity of the trajectories of individual loci, collective motions of chromatin are seen to be coherent beyond the boundaries of chromosome territories, over micrometer-scale regions; this suggests that there is some sort of mechanical coupling between loci very far apart along the polymer or even belonging to two different polymers (4, 5). The medium surrounding the chromosomes is also believed to be viscoelastic on the basis of the velocity autocorrelation functions of fluorescently labeled loci, which show a characteristic negative dip (3). These results have been rationalized using several heuristic pictures, including models that describe the motions of loci as those of individual particles in a complex effective medium (e.g., see refs. 6 and 7), various polymer dynamics models based on continuum pictures (e.g., see refs. 8–10), and more recently, by including in the polymer model general features about the folding of chromosomes (11).

In this article, we characterize the motions of chromosomal loci using an energy landscape model [the minimal chromatin model (12)] that was originally derived to account for the spatial folding of the genome as quantified by the contact probabilities measured by Hi-C (13). We show here that the very same interactions that account for the structural aspects of genome organization in interphase also naturally give rise to the main temporal features of genome dynamics that have so far been discussed in the experimental literature. Additionally, we introduce the notion of dynamically associated domains (DADs), i.e., spatial domains where chromatin tends to move coherently, and we characterize their behavior using the information provided by detailed molecular dynamics simulations.

Many aspects of chromatin spatial organization in interphase have become evident through the use of DNA–DNA ligation assays. Most prominent of these are looping and compartmentalization (13, 14). A chromatin loop (or a link) is created when two loci form a particularly strong contact, which then appears as a local peak in the experimental contact probability map (14). Most of these special genomic contacts are intrachromosomal (and therefore referred to as "loops") and are associated with the presence of CCCTC-binding factor (CTCF) and cohesin. There

Significance

Several active processes operate on eukaryotic genomes, dictating their three-dimensional arrangement and dynamical properties. The combination of structural organization and dynamics is essential to the proper functioning of the cell. We show that an effective energy landscape model for chromatin provides a unifying description of both the structural and dynamical aspects of the genome, recapitulating many of its features. Using this quasi-equilibrium energy landscape model, we demonstrate that the physical interactions accounting for genome architecture also lead to the nontrivial dynamical behavior of genomes previously described in multiple experimental observations.

Author contributions: M.D.P., D.A.P., P.G.W., and J.N.O. designed research, performed research, contributed new reagents/analytic tools, analyzed data, and wrote the paper.

Reviewers: O.K.D., University of California, San Diego; and A.J.S., Stanford University.

The authors declare no conflict of interest.

This open access article is distributed under Creative Commons Attribution-NonCommercial-NoDerivatives License 4.0 (CC BY-NC-ND).

[1]M.D.P. and D.A.P. contributed equally to this work.

[2]To whom correspondence may be addressed. Email: Michele.DiPierro@rice.edu or jonuchic@rice.edu.

This article contains supporting information online at www.pnas.org/lookup/suppl/doi:10.1073/pnas.1806297115/-/DCSupplemental.

Published online July 9, 2018.

also exist, however, strong intrachromosomal contacts in the absence of CTCF or cohesin as well as strong interchromosomal contacts (referred to as "links") associated with the presence of superenhancers and bound transcription factors (15). Another key feature of chromatin architecture, in our view, is the tendency of chromatin to exhibit liquid crystalline order, a tendency that becomes dominant in the metaphase chromosome (12, 16, 17). In addition to these features chromatin turns out to be compartmentalized (13).

A model for chromatin folding [the minimal chromatin model or MiChroM (12)] that incorporates all of these features argues that compartmentalization arises from microphase separation of chromatin segments having different biochemical properties. Quantifying the correlations between compartmentalization and epigenetic markings leads to a predictive energy landscape with transferable interactions. The interactions between locally encoded types of chromatin turn out to be sufficient to predict the specific patterns of compartmentalization in genomes (18).

Together with the compartmentalization of chromosomes coming from contact interactions, MiChroM also regards the local structure of the chromatin polymer and the CTCF-mediated looping interactions as coming from direct interactions in space that ultimately are mediated by proteins, about whose identity and activity the model remains however agnostic. The quasi-equilibrium effective energy landscape (19) provided by MiChroM generates 3D chromosomal structural ensembles, whose contact maps agree in detail with those found by ligation assays (Hi-C). The ensembles also are consistent with the results from fluorescence in situ hybridization (FISH) studies that mark locations in 3D space (18).

In MiChroM the genome architecture (in interphase) is encoded in the one-dimensional sequence of epigenetic markings and loops much as 3D protein structures are determined by their 1D sequence of amino acids and by the position of disulfide bonds (Fig. 1*A*). In contrast to the situation for proteins, however, the sequence code provided by the epigenetic marks is not fixed but is dynamically rewritten during cell differentiation, modulating both the 3D structure and gene expression in different cell types. Under the regulation of the epigenetic markings, proteins act to generate the quasi-equilibrium energy landscape shaping the genomic conformational ensemble. In this ensemble, some contacts are transient and short-lived, like the ones leading to compartmentalization, while others, like those related to CTCF for example, are strong and long lasting. In the latter case, experimental data indicate lifetimes that span from minutes to tens of hours (20).

Here, we revisit the results of several experimental observations regarding chromatin dynamics in the light of the quasi-equilibrium landscape theory for genome structural organization outlined above. The simulations of the energy landscape of chromosomes, in addition to recapitulating their structural ensembles, turn out to reproduce also the main dynamical observations: anomalous diffusion, viscoelasticity, and spatially coherent dynamics.

Subdiffusivity and Viscoelasticity

The transport of individual biomolecules is usually modeled as occurring through Brownian diffusion. Ordinary diffusion of a single particle leads to ergodic, self-similar trajectories in which the mean-square displacement shows linear scaling with the time τ over which the displacement is observed ($\langle (r(t+\tau)-r(t))^2 \rangle \sim \tau$). Multiple experiments on chromatin dynamics, however, report significant deviations from the simple one-particle diffusive behavior. In mammalian cells, Bronstein et al. (2) found that the motion of telomeres is initially subdiffusive with mean-square displacement scaling as τ^{α} with the rather small exponent $\alpha = 0.3$ for much of the observed time course. Only in the long time limit do the displacements begin to transition into a regime describable as normal diffusion. In bacterial cells, the trajectories in the experiments from Weber et al. (9) gave an α exponent of about 0.4. Depleting the ATP of the cell slows down active processes and significantly reduces the diffusion constant but apparently leaves unchanged the subdiffusive scaling, suggesting that ATP-dependent enzymatic activity somehow contributes to molecular agitation but is not the origin of the subdiffusive nature of the displacements (1).

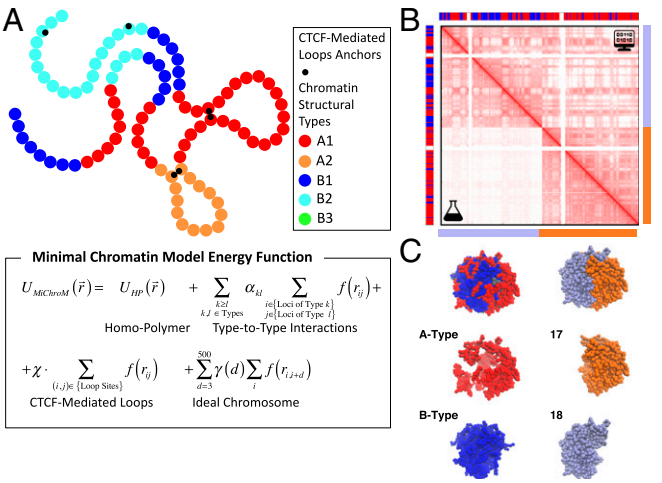

Fig. 1. The MiChroM. (*A*) A schematic representation of the MiChroM together with its information theoretic energy function (12). The model accounts for genome organization through a homopolymeric potential plus contact interactions of three kinds: differential interactions between chromatin structural types (loci belonging to different types are here represented with different colors), CTCF-mediated looping interactions (the anchors of these loops are represented by the black dots), and the interactions modeling the liquid crystalline behavior of chromatin contained in the Ideal chromosome potential. (*B*) The contact matrix shows the probability of observing a contact between loci *i* and *j*, p_{ij}. Experimentally determined values for the contact probability from Hi-C (14) are shown in the lower triangular section of the matrix while theoretically predicted results are shown in the upper triangular section. Sidebars indicate the A/B type annotations of the locus (in red and blue, respectively) and the locations of the two simulated chromosomes (chromosome 17 in orange and 18 in lavender). The evident symmetry of the matrix indicates the accuracy of the predictions. Enhanced frequencies of interchromosomal contacts in simulations are due to the effects of confinement, as discussed in ref. 12. (*C*) A typical configuration extracted from the simulated trajectories. Chromosomes show microphase separation of chromatin types (left-hand column), and territorialization (right-hand column) with each chromosome occupying nonoverlapping regions of space.

The connectivity of the chromosomal polymer chain reduces the amount of space explored by the monomers composing the biopolymer and could therefore be one of the causes of the subdiffusive behavior. Several models of polymer dynamics do indeed give rise to subdiffusive behavior. de Gennes's reptation model of chains confined in tubes predicts very slow diffusion with a scaling exponent $\alpha = 0.25$, while freely connected chain diffusion in the Rouse model leads to $\alpha = 0.5$, and when the hydrodynamic streaming is accounted for by Zimm's model yields an exponent $\alpha = 0.67$.

The anomalous diffusion of genomic loci has also been variously ascribed to the viscoelastic nature of medium surrounding the chromosomes, the transient binding/unbinding of proteins, and to obstructed diffusion. Likely, all of these factors may operate in the nucleus of eukaryotic cell. Phenomenological descriptions to account for such effects include fractional Brownian motion, continuous time random walks, and obstructed diffusion models (2, 6, 7). These phenomenological models can describe the motions of

individual tracked particles but cannot describe the spatial structure or coherence of the motions. The high-dimensional energy landscape encoded in the MiChroM contains elements of all these qualitative phenomena. The MiChroM landscape, by being polymeric, includes chain connectivity, but also encodes the structural effects of transient binding of proteins and the obstructed diffusion of loci due to steric interactions of one part of the chain with other parts.

Transient binding of proteins determines the number and the strength of the protein-mediated cross-links, which affect the diffusion of individual loci. Bronshtein et al. (21) found that depleting protein lamin A leads to much faster diffusion. While Lamin A is not explicitly accounted for in the MiChroM landscape, the intensity of cross-linking present in MiChroM is determined by the thermodynamical interpretation of the in situ structural data provided by Hi-C and therefore to some extent may include also the effect of this specific protein.

In this paper we focus on simulating the dynamics of chromosomes 17 and 18 of human lymphoblastoid cells. These simulations employ dynamics generated by a Langevin equation for the chain moving on the MiChroM energy landscape. No large steps, as might arise from far from equilibrium motors, are allowed in the algorithm. Such steps could give rise to active flows (22).

As already observed in ref. 12, the intrachromosomal contact maps obtained by these simulations closely reproduce the maps obtained from the DNA–DNA ligation assays (14), indicating that the structural ensemble of the chromosomes is reasonably well reproduced (Fig. 1*B*). The 3D structural ensemble exhibits phase separation of chromatin structural types that extends to both chromosomes, creating regions of space occupied by one single chromatin type but coming from both chromosomes (Fig. 1*C*). We also found that, despite there being extensive spatial contacts between the chromosomes, distinct chromosomes themselves do not become topologically entangled with one another; instead, the landscape leads to the formation of nonoverlapping chromosome territories (Fig. 1*C*).

The quasi-equilibrium Langevin simulations lead to a scaling exponent of 0.29 for the mean-square displacement of the telomeres in 3D space (Fig. 2). This exponent value is consistent with the experimental results reported by Bronstein et al. (2) for other human cells (osteosarcoma cell line U2OS) (Fig. 2). The velocity autocorrelation functions $C_v^{\delta}(\tau) = \langle v(t+\tau) \cdot v(t) \rangle$ with $v(t) = 1/\delta(r(t+\delta) - r(t))$ obtained from the simulations reveal a negative correlation at characteristic relaxation time scales (23). We see the chromosome behaves as if it were viscoelastic (Fig. 3*A*). Identical viscoelastic behavior was observed in vivo by Lucas et al. (3) in mammalian cells. The simulated velocity autocorrelation functions measured for different time lags, when rescaled by the corresponding time lag δ, all collapse to a universal curve, indicating self-similarity of motion. The experimental data also collapse in the same universal fashion (3).

MiChroM contains no explicit viscoelastic medium or dynamical memory kernel; instead, the memory and elasticity come from the chains and their interactions. At the bead level the motion does actually start out as a simple diffusion, as dictated by the Langevin equation, but the motion then becomes slower because of the interactions between loci encoded in MiChroM. In making comparisons of the simulations with experiments, the unit of length in our simulation was previously calibrated using FISH (18). The unit of time was chosen to reproduce the free passive diffusive properties of loci (i.e., the beads of the model) in pure water treated hydrodynamically at room temperature (*SI Appendix*). As we shall see, hydrodynamic diffusion is slowed but in discussing the comparisons between theory and experiments below no further adjustable quantity is needed to fit the experimental data. The viscoelasticity manifested by the chromosomal loci

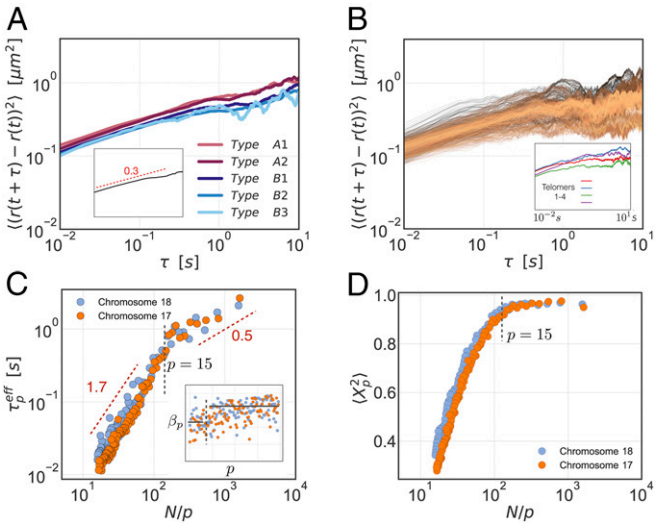

Fig. 2. Anomalous diffusion in chromatin. (*A*) The mean-square displacements predicted by the simulations for the different chromatin structural types. (*Inset*) Average over all loci and its power-law fit. In simulated trajectories for the human lymphoblastoid cells (GM12878), the mean-square displacement scales as τ^{α} with an exponent $\alpha = 0.29$, indicating a markedly subdiffusive behavior. The predicted diffusive exponent compares favorably with what was previously reported for other human cell lines (ref. 2 reports $\alpha = 0.3$ for the osteosarcoma cell line U2OS) and bacterial cells (ref. 9 reports $\alpha = 0.4$ for *Escherichia coli* and *Caulobacter*). (*B*) The square displacements of single loci are shown with different colors as a function of time. (Inset) Mean-square displacements for the four telomeres are shown. The heterogeneity of simulated trajectories compares favorably with what was noted in refs. 2 and 3, while ref. 9 reports an even higher amount of heterogeneity. The predicted diffusivity from simulations is higher than what is reported in experiments, indicating that loci in the MiChroM move faster than what is observed in vivo through microscopy. This may be related to a variety of causes, including an incorrect estimation of the viscosity of the nuclear environment or the underestimation of the intensity of cross-linking in chromatin. (*C*) Effective relaxation times of Rouse modes for the polymeric chains of the chromosomes. (*Inset*) Exponents β_p of the stretched exponential relaxation function fits to the mode correlation functions. The two horizontal lines correspond to $\beta_p = 0.6$ and $\beta_p = 0.8$, the vertical line corresponds to $p = 15$. (*D*) Scaling of the amplitudes of Rouse modes for the chromosome chains. Two distinct regimes are clearly visible in both *C* and *D*.

displacements together with the specific subdiffusive dynamics of individual locus motion apparently emerge directly from the same physical mechanisms that lead to the spatial organization of the genome.

The trajectories of different loci in vivo are known to be highly heterogeneous. The square displacements of different loci at the 1-s time interval are scattered over a range of values spanning one (2, 3) or even two orders (9) of magnitude. The MiChroM simulations also display heterogeneity, with displacements at the same time ranging over almost one order of magnitude, thus somewhat smaller than the experimentally observed scatter (Fig. 2*B*). On the other hand, the purely hydrodynamic model of the bead friction overestimates the diffusivity over what is seen experimentally. At the 1-s mark, simulations show loci displacements ranging from 10^{-1} to 1 μm, while in the same time interval displacements are observed in vivo to comprise the range 10^{-3}–10^{-1} (9) (Fig. 2 *A* and *B*). The far from equilibrium activity of motor proteins, which cannot be accounted for by the quasi-equilibrium energy landscape of MiChroM, is a possible explanation for the higher heterogeneity of the trajectories observed experimentally. Additional cross-linking that does not show up in the Hi-C data might also contribute to this heterogeneity, as well as significantly affect the diffusive properties of chromosomal loci (21).

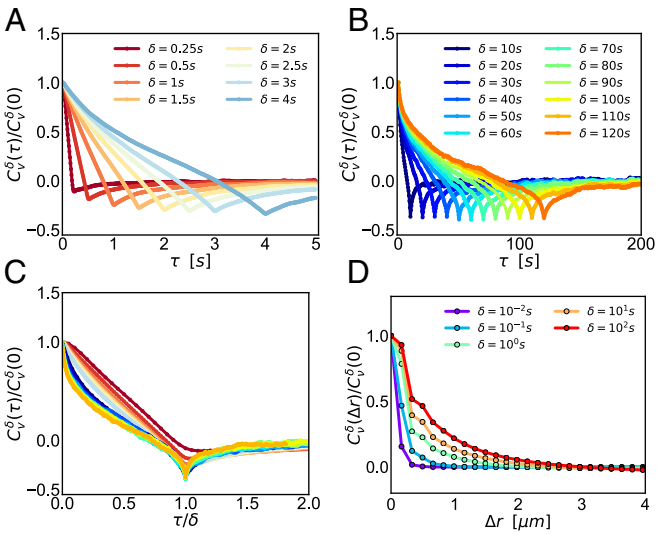

Fig. 3. Viscoelastic behavior in chromatin. (*A* and *B*) Velocity autocorrelation functions $C_v^\delta(\tau) = \langle v(t+\tau)\cdot v(t)\rangle$with $v(t) = 1/\delta(r(t+\delta) - r(t))$ obtained from the simulations for different time intervals δ and plotted as a function of the time delay τ. We see the chromosome behaves as a viscoelastic medium. The same viscoelastic behavior was observed in vivo by Lucas et al. (3) in mammalian cells. Curves for the shortest time scales, shown in *A*, deviate from exact self-similarity, with a deepening negative peak. This behavior, not seen in experiments, is an artifact of the Langevin dynamics integrator, whose damping time corresponds to 1 s and is therefore comparable to the shorter time scales tested. Curves corresponding to longer time intervals, shown in *B*, are instead markedly self-similar. The negative peak stabilizes at a value of −0.375. Global confinement would give a value of −0.5 (25). Interestingly, the value −0.375 is quite similar to the experimentally determined value in ref. 3. (*C*) The simulated velocity autocorrelation functions measured for different time lags, when rescaled by their time lag δ, collapse reasonably well to a single curve. Experimental data collapse in the same universal fashion (3). (*D*) Velocity correlations of loci $C_v^\delta(\Delta r) = \langle v(r_i(t),\delta)\cdot v(r_j(t),\delta)\delta(|r_i(t) - r_j(t)| - \Delta r)\rangle$ as a function of the scalar distance in space between the loci, Δr, and for different time lags δ. Simulations show that spatial coherence increases when one increases the time lag in observations. Similar behavior was seen for correlations in HeLa cells in ref. 4. The coherence of motion in the simulated conformational ensembles increases monotonically over time lags δ spanning four orders of magnitude. The size of the correlated region is predicted to be on the micrometer scale, once again comparing favorably with what is seen in the laboratory (4).

To uncover the origin of the dynamics and correlated motions in the chain we calculated the relaxation times for the Rouse modes of the chromosome chains. For a simply connected chain without excluded volume or hydrodynamic interactions the Rouse picture leads to overdamped vibrational modes. These modes correspond to the vibrations of the polymeric chain and are labeled by their inverse wavelength. For harmonic chains the modes are independent of each other and uncorrelated. Their individual correlation functions are expected to decay as simple exponentials; for each mode of wavenumber p we expect $\langle \overrightarrow{X_p}(t)\overrightarrow{X_p}(0)\rangle = \langle \overrightarrow{X_p^2}\rangle e^{-t/\tau_p}$ and $\langle \overrightarrow{X_p^2}\rangle \sim p^{-2}$. The dynamics of real chains, however, deviates from predictions of the Rouse model, which only treats the interactions along the chain. There are contributions from excluded volume effects, intramolecular bond correlations, chain stiffness, confinement, and tertiary interactions. Our simulations reveal, contrary to the predictions of the free-chain Rouse theory, that the correlation functions of the Rouse modes of the simulated chromosomes are individually best fit by stretched exponential functions $\langle \overrightarrow{X_p}(t)\overrightarrow{X_p}(0)\rangle \sim A_p e^{-(t/\tau_p)^{\beta_p}}$ with exponents β_p varying between 0.4 and 1, and typically increasing with the mode number (Fig. 2*C*, *Inset*). This complex decay of even a single mode reveals there is a nontrivial hierarchy of relaxation time scales (24) (Fig. 2 *C* and *D*). The scaling of relaxation times with the mode number is also more complex than predicted for the free chain. The effective relaxation times of the vibrational modes in the simulations, which can be quantified through a time integral over the relaxation function as $\tau_{eff} = \int_0^\infty e^{-(t/\tau_p)^{\beta_p}} = \tau_p/\beta_p\Gamma(\beta_p^{-1})$, deviate from those of the idealized Rouse dynamics that predicts the universal scaling $\tau_{eff} \sim p^{-2.0}$. In MiChroM, the observed scaling of the effective relaxation times with the mode number is $\tau_{eff} \sim p^{-0.5}$ for the long-wavelength modes (P = 1–15) but do follow approximately Rouse behavior having $\tau_{eff} \sim p^{-1.7}$ for the shorter-wavelength modes (P = 15–100).

Similarly, the amplitudes of the Rouse modes of the simulated chains also deviate from the free-chain prediction. Once again, the deviations from the Rouse theory are seen in longer-wavelength modes (Fig. 2*D*).

Overall, the analysis of the correlations reveals two distinct regimes. While the short-wavelength modes are reasonably well approximated by the free chain, the behavior of the first 10–20 modes, which are long in wavelength, deviates quite significantly from the free-chain model. In the next paragraph, in analyzing the motions of chromatin in simulations, we provide evidence suggesting that these deviations from the Rouse picture originate from the coherent motion of dynamically associated domains.

Spatial Coherence, Compartmentalization, and Microphase Separation

Zidovska et al. were able to map the projected motion of chromatin simultaneously across the whole nucleus of human cells to generate a 2D vector field of chromatin displacements (4). The analysis of the resulting projected displacement field shows that the motion of chromatin is coherent across large regions for several seconds. The regions of coherence extend over the micrometer scale and cross the boundaries of chromosome territories. When ATP is depleted the coherent motion is eliminated, indicating that such coherence results from protein activity.

Fig. 4 shows the 3D displacement fields predicted by MiChroM. The map shows the existence of coherent motion, in a way that parallels the experimental maps, noting however that in the simulations the data do not need to be projected into two dimensions as was done in experiments. The velocity fields $v(r_i(t),\delta) = 1/\delta(r_i(t+\delta) - r_i(t))$ obtained for different time lags δ are shown for comparison in Fig. 4*A*. As in the experiments, it is evident that coherence grows for longer time lags. Fig. 3*B* shows the velocity correlation $C_v^\delta(\Delta r) = \langle v(r_i(t),\delta)\cdot v(r_j(t),\delta)\delta(|r_i(t) - r_j(t)| - \Delta r)\rangle$ as a function of the spatial displacement Δr and for different time lags δ.

The boundaries between the regions of coherent motions seen in simulations are not the same as the boundaries between the chromosomal territories that are occupied by chromosomes 17 and 18. One easily verifies this observation by inspecting the matrix of the velocity correlations $c_{ij}(t,\delta) = v(r_i(t),\delta)\cdot v(r_j(t),\delta)$ between loci i and j (Fig. 4*B*) and comparing it to the structural map. In the matrix of velocity correlations one can observe once again that coherence grows for longer time lags, as the domains of coherent motion encompass larger chromosomal regions for larger time lags δ.

The boundaries of the coherent regions appear to change stochastically through thermal fluctuations; at times a particularly weak interface can be created, allowing reconfiguration. In simulations, according to our model, these weaker interfaces are defined by the three kinds of interactions present in the Hamiltonian, i.e., chain connectivity, soft-core repulsive interactions, and the "stickiness" that models the effect of protein-mediated

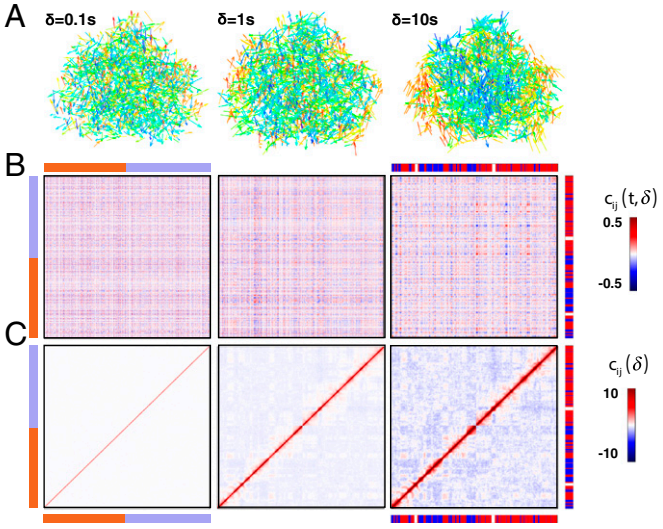

Fig. 4. Coherent motion in chromatin. (*A*) The 3D vector field of loci velocities $v(r,t)=1/\delta(r(t+\delta)-r(t))$ for a typical configuration at time *t*. Velocities are measured over increasing time intervals $\delta$from left to right. The color of the arrows indicates the direction of the velocity vector, with red marking the outward-oriented *z* axis. It is visually evident that increasing the time interval increases the size of the regions of coherent motion. This result is qualitatively similar to what was observed in ref. 4. (*B*) Matrix of the instantaneous velocity correlations $c_{ij}(t,\delta)=v(r_i(t),\delta)\cdot v(r_j(t),\delta)$ between loci *i* and *j* for a typical configuration at time *t* and for increasing time intervals δ. The color of a pixel indicates the instantaneous velocity correlation increasing from blue to red. The sidebars indicate chromatin structural type annotations (type A in red and B in blue) and chromosome identity (chromosome 17 in orange and 18 in lavender). The regions of coherence increase in size as indicated by the coarsening of the plaid pattern when moving from left to right, as one increases the coarse-graining time interval δ. (*C*) Ensemble-averaged matrix of the velocity correlations $c_{ij}(\delta)=\langle v(r_i(t),\delta)\cdot v(r_j(t),\delta)\rangle$ between loci *i* and *j*, for increasing time intervals δ. The color of each pixel indicates the average velocity correlation increasing from blue to red. Regions of correlated motion often align with the biochemical properties of the phase-separated chromatin as indicated by the alignment of the patterns with the chromatin structural type annotations on sidebars. The dominant features of the matrices change as the time lag δincreases. For $\delta=0.1s$ only correlations due to chain connectivity are visible strictly along the diagonal of the matrix. As δincreases we see large correlations spreading away from the diagonal; these correlations indicate the coherent motion of TADs. Off the diagonal one also starts to see the weaker correlations due to phase separation. Lastly, on the very longest time scales one can also see the correlations associated with chromosomal territories becoming visible in the matrix on the right-hand side for $\delta=10$ s and in the matrix for $\delta=100$ s shown in *SI Appendix*, Fig. S7.

crosslinking. The MiChroM explains the formation of spatial chromosomal compartments through a process of microphase separation of chromatin sharing similar epigenetic marking patterns. Segments of similarly marked chromatin are brought together by their differential stickiness, modeling the effect of protein-mediated contact interactions. These contact interactions generate an energy landscape in which chromatin of the same kind segregates into liquid droplets that retain some identity dynamically.

By averaging the matrix of the velocity correlations between genomic loci over the ensemble of structures, $c_{ij}(\delta)=\langle v(r_i(t),\delta)\cdot v(r_j(t),\delta)\rangle$, we smooth out the noise to analyze the qualitative elements of the dynamics generated by MiChroM (Fig. 4*C*).

The dominant features of the matrices of the ensemble-averaged pairwise velocity correlations $c_{ij}(\delta)$ differ at the various time lags δ, which represent the degree of temporal coarse graining over which the velocity field is calculated. For short intervals of time separation, δ, only the correlations due to chain connectivity can be easily seen, strictly manifested along the diagonal of the matrix. Loci that sit close along the chain tend to move coherently. For correlations at longer time intervals, one sees, arising somewhat further away from the diagonal, additional domains of coherence that apparently are related to the motion of dynamically associated domains.

These DADs, much as do their structural counterparts topologically associated domains (TADs), often align with the A/B chromatin-type annotation. Off the diagonal, the velocity correlation map does exhibit weaker correlations due to phase separation; this indicates that domains belonging to the same chromatin type often segregate in the same liquid droplet and therefore show, on average, more coherence than otherwise. Lastly, on the very longest time scales one uncovers dynamical correlations associated with chromosomal territories (*SI Appendix*, Fig. S6).

Each of the two chromosomes contains roughly 10–20 DADs, suggesting that the coherence of the motion of DADs is indeed responsible for the significant deviations found in the first 10–20 long-wavelength vibrational modes between the simulated chromosomes and the continuum theoretical predictions.

A similar analysis can also be carried out using the matrices of the velocity correlations between genomic loci with a time delay Δt, $c_{ij}(\delta,\Delta t)=\langle v(r_i(t),\delta)\cdot v(r_j(t+\Delta t),\delta)\rangle$; in these matrices (*SI Appendix*, Fig. S7) we see a more detailed version of the negative correlation dip seen in the one-dimensional velocity autocorrelation plot. The positive correlations, on and off the diagonal, quickly decay with increasing Δt. Successively, chain connectivity generates a negative velocity correlation between neighbors, which then spreads to the DADs along the diagonal.

Due to the unavailability of assays combining correlation spectroscopy with knowledge of the genomic identity of the tracked loci, these predictions concerning the relation between dynamics and structure coming from the MiChroM energy landscape about the origin of the coherence remain to be tested in the laboratory.

Conclusion

It is not immediately obvious whether the same energy landscape that describes the structural ensemble would also be adequate to describe the dynamics. Nevertheless, if the step sizes of the motions induced by the nonequilibrium engines are smaller than the characteristic length scales of the forces, it has been shown that an active motorized system can still be described as a quasi-equilibrium system with a renormalized temperature and diffusion coefficient as has been discussed in the context of cytoskeleton models (22). If instead the step sizes are larger than the range of the forces, vectorial flows can develop which would be missing from a Langevin simulation using a quasi-equilibrium landscape description of the system. In this article we have analyzed the motion of the human chromosomes predicted by a quasi-equilibrium landscape that fits accurately the known structural data. Remarkably, the quasi-equilibrium landscape description turns out to be compatible with numerous dynamical observations of the chromosomes in vivo. The very same interactions that account for 3D organization of the genome in interphase seem to reproduce naturally several nontrivial features of the genome's four-dimensional dynamics, namely, the spatial coherence of mobile regions, the subdiffusive nature of the trajectories of individual loci, and the apparent viscoelastic nature of chromatin itself.

ACKNOWLEDGMENTS. M.D.P. and D.A.P. thank Ryan R. Cheng and Vinicius Contessoto for many useful conversations. This work was supported by the Center for Theoretical Biological Physics sponsored by National Science Foundation (NSF) Grant PHY-1427654. J.N.O. was also supported by the NSF Grant CHE-1614101 and by the Welch Foundation (Grant C-1792). Additional support to P.G.W. was provided by the D. R. Bullard-Welch Chair at Rice University (Grant C-0016).

1. Weber SC, Spakowitz AJ, Theriot JA (2012) Nonthermal ATP-dependent fluctuations contribute to the in vivo motion of chromosomal loci. *Proc Natl Acad Sci USA* 109: 7338–7343.
2. Bronstein I, et al. (2009) Transient anomalous diffusion of telomeres in the nucleus of mammalian cells. *Phys Rev Lett* 103:018102.
3. Lucas JS, Zhang Y, Dudko OK, Murre C (2014) 3D trajectories adopted by coding and regulatory DNA elements: First-passage times for genomic interactions. *Cell* 158:339–352.
4. Zidovska A, Weitz DA, Mitchison TJ (2013) Micron-scale coherence in interphase chromatin dynamics. *Proc Natl Acad Sci USA* 110:15555–15560.
5. Shaban HA, Barth R, Bystricky K (2018) Formation of correlated chromatin domains at nanoscale dynamic resolution during transcription. *Nucleic Acids Res,* 10.1093/nar/gky269.
6. Metzler R, Jeon JH, Cherstvy AG, Barkai E (2014) Anomalous diffusion models and their properties: Non-stationarity, non-ergodicity, and ageing at the centenary of single particle tracking. *Phys Chem Chem Phys* 16:24128–24164.
7. Sokolov IM (2012) Models of anomalous diffusion in crowded environments. *Soft Matter* 8:9043–9052.
8. Lampo TJ, Kennard AS, Spakowitz AJ (2016) Physical modeling of dynamic coupling between chromosomal loci. *Biophys J* 110:338–347.
9. Weber SC, Spakowitz AJ, Theriot JA (2010) Bacterial chromosomal loci move subdiffusively through a viscoelastic cytoplasm. *Phys Rev Lett* 104:238102.
10. Weber SC, Theriot JA, Spakowitz AJ (2010) Subdiffusive motion of a polymer composed of subdiffusive monomers. *Phys Rev E Stat Nonlin Soft Matter Phys* 82:011913.
11. Polovnikov KE, Gherardi M, Cosentino-Lagomarsino M, Tamm MV (2018) Fractal folding and medium viscoelasticity contribute jointly to chromosome dynamics. *Phys Rev Lett* 120:088101.
12. Di Pierro M, Zhang B, Aiden EL, Wolynes PG, Onuchic JN (2016) Transferable model for chromosome architecture. *Proc Natl Acad Sci USA* 113:12168–12173.
13. Lieberman-Aiden E, et al. (2009) Comprehensive mapping of long-range interactions reveals folding principles of the human genome. *Science* 326:289–293.
14. Rao SSP, et al. (2014) A 3D map of the human genome at kilobase resolution reveals principles of chromatin looping. *Cell* 159:1665–1680.
15. Rao SSP, et al. (2017) Cohesin loss eliminates all loop domains. *Cell* 171:305–320.e24.
16. Zhang B, Wolynes PG (2016) Shape transitions and chiral symmetry breaking in the energy landscape of the mitotic chromosome. *Phys Rev Lett* 116:248101.
17. Zhang B, Wolynes PG (2015) Topology, structures, and energy landscapes of human chromosomes. *Proc Natl Acad Sci USA* 112:6062–6067.
18. Di Pierro M, Cheng RR, Lieberman Aiden E, Wolynes PG, Onuchic JN (2017) De novo prediction of human chromosome structures: Epigenetic marking patterns encode genome architecture. *Proc Natl Acad Sci USA* 114:12126–12131.
19. Zhang B, Wolynes PG (2017) Genomic energy landscapes. *Biophys J* 112:427–433.
20. Hansen AS, Cattoglio C, Darzacq X, Tjian R (2018) Recent evidence that TADs and chromatin loops are dynamic structures. *Nucleus* 9:20–32.
21. Bronshtein I, et al. (2015) Loss of lamin A function increases chromatin dynamics in the nuclear interior. *Nat Commun* 6:8044.
22. Wang S, Wolynes PG (2011) On the spontaneous collective motion of active matter. *Proc Natl Acad Sci USA* 108:15184–15189.
23. Zhang Y, Dudko OK (2016) First-passage processes in the genome. *Annu Rev Biophys* 45:117–134.
24. Padding JT, Briels WJ (2002) Time and length scales of polymer melts studied by coarse-grained molecular dynamics simulations. *J Chem Phys* 117:925–943.
25. Weber SC, Thompson MA, Moerner WE, Spakowitz AJ, Theriot JA (2012) Analytical tools to distinguish the effects of localization error, confinement, and medium elasticity on the velocity autocorrelation function. *Biophys J* 102:2443–2450.